13.C.2 ENVIRONMENTAL HUMIDITY, OUTER-CORE PRECIPITATION, AND TROPICAL CYCLONE SIZE

Gary M. Lackmann* and Kevin A. Hill
North Carolina State University, Raleigh, North Carolina

1. INTRODUCTION

Tropical cyclones (TCs) are observed to span a large range of sizes; these differences are evident in the size of the eye as well as in the lateral extent of the wind, cloud, and precipitation fields. Previous studies have demonstrated that the size of a TC wind field can vary with ocean basin, time of year, latitude, minimum central pressure, stage of development, and environmental pressure (Atkinson 1971; Frank and Gray 1980; Merrill 1984; Cocks and Gray 2002; Kimball and Mulekar 2004).

The size of a TC has obvious connections with TC impacts, including storm surge, precipitation amount, area impacted by damaging winds, and the area threatened by tornadoes subsequent to landfall. Nevertheless, few studies have examined the physical mechanisms that determine TC size. Merrill (1984) hypothesized that changes in the TC size were related to angular momentum imports resulting from latitudinal changes or changes in synoptic environment. Emanuel (1986) and Rotunno and Emanuel (1987) highlighted the size of the initial disturbance as a determining factor. A more recent study by Kimball (2006) found that model TCs initialized within a larger envelope of moisture developed into larger storms relative to those initialized within a smaller moist envelope, although the physical mechanism responsible for this difference in size was not investigated.

We hypothesize that the size of a TC is related to the intensity and coverage of precipitation outside the radius of maximum wind (RMW), which is in turn related to environmental relative humidity. From a potential vorticity (PV) perspective, the size of the balanced primary circulation in a TC is linked to the size and strength of cyclonic PV anomalies associated with the storm. Lateral growth of the lower-tropospheric PV in response to latent heat release in outer rainbands results in lateral expansion of the cyclonic PV tower.

Corresponding author address: Gary Lackmann, Dept. of Marine, Earth, & Atmospheric Sciences, 1125 Jordan Hall, Box 8208, Raleigh NC 27695-8208. E-mail: gary@ncsu.edu

Heavier precipitation in spiral bands outside the RMW favors a larger lateral extent of the PV tower and wind field. PV arguments are consistent with other viewpoints in that the pressure and rotational wind fields are linked through gradient balance.

The hypothesis is tested using a series of idealized TC simulations in which the environmental relative humidity is varied. Dry initial environments tend to inhibit precipitation in outer portions of the TC, which should result in a narrower PV tower and smaller RMW, whereas more moist environments are conducive to greater precipitation at larger radii, a broader PV tower, and larger lateral extent of the TC wind field. We recognize that the lateral precipitation distribution can be sensitive to other factors besides environmental relative humidity, such as frontal or trough interactions and topographic forcing. However, changing the environmental relative humidity in idealized simulations provides a straightforward means of testing our primary hypothesis.

2. MODEL CONFIGURATION

Version 2.2 of the Weather Research and Forecasting model (WRF-ARW, Skamarock et al. 2007) was used to conduct four idealized model experiments designed to investigate the sensitivity of TC size to environmental humidity. High resolution explicit convection simulations (2-km horizontal grid spacing, 47 vertical levels) were utilized in order explicitly represent the grid-scale heating profile, which is needed to examine the hypothesis that outer-core latent heating was associated with the cyclonic PV tower expansion. The WSM6 microphysics scheme (Hong and Lim 2006) and Mellor-Yamada-Janjić turbulence scheme (Janjić 2002) were employed in these simulations.

A weak warm-core vortex (maximum wind speed ~17 m s^{-1}) in hydrostatic and gradient wind balance was inserted in a horizontally uniform base state, as in Hill and Lackmann (2008). Environmental temperatures were obtained from the mean tropical sounding of Jordan (1958), and

the SST was specified at a constant value of 29°C. To investigate the sensitivity of simulated TC size to the environmental moisture content, four otherwise identical model experiments were performed, with relative humidity values of 80, 60, 40 and 20% defined with respect to liquid water, applied uniformly in the model initial conditions. These model simulations are hereafter referred to as 80RH, 60RH, 40RH, and 20RH, respectively.

The idealized experiments were conducted using the full-physics version of WRF on an actual geophysical domain, but with the domain set to include only water. The vortex-tracking moving nest feature was utilized in the simulations. The initial vortex was centered at 10°N, although additional experiments reveal that the results are not sensitive to this choice (not shown). Model simulations were run for 10 days, which allowed the storms to attain a quasi-steady intensity.

3. SIMULATION RESULTS

The simulated TCs in the 20RH and 40RH runs attain a minimum central pressure of ~910 hPa, while the TCs in the 60RH and 80RH runs reach ~900 hPa and ~885 hPa, respectively (Fig. 1). Despite lower minimum surface pressure values, the TCs in the more moist simulations are larger in size, yielding comparable gradient wind magnitudes and similar maximum wind speeds (not shown).

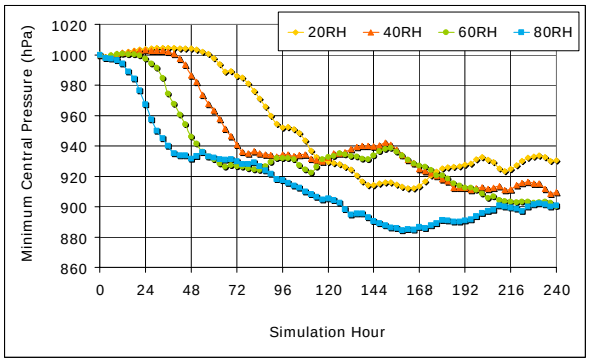

Figure 1. Minimum central sea-level pressure time series. Simulation indicated in legend.

The initial rate of intensification is sensitive to the initial environmental humidity, with rapid intensification delayed by over 2 days in the 20RH simulation relative to the 80RH run (Fig. 1). Due to our use of horizontally uniform RH in the initial conditions, considerable moistening of the environment due to turbulent fluxes and convection is required prior to rapid intensification of the simulated TCs, especially in the dry simulations (Fig. 2).

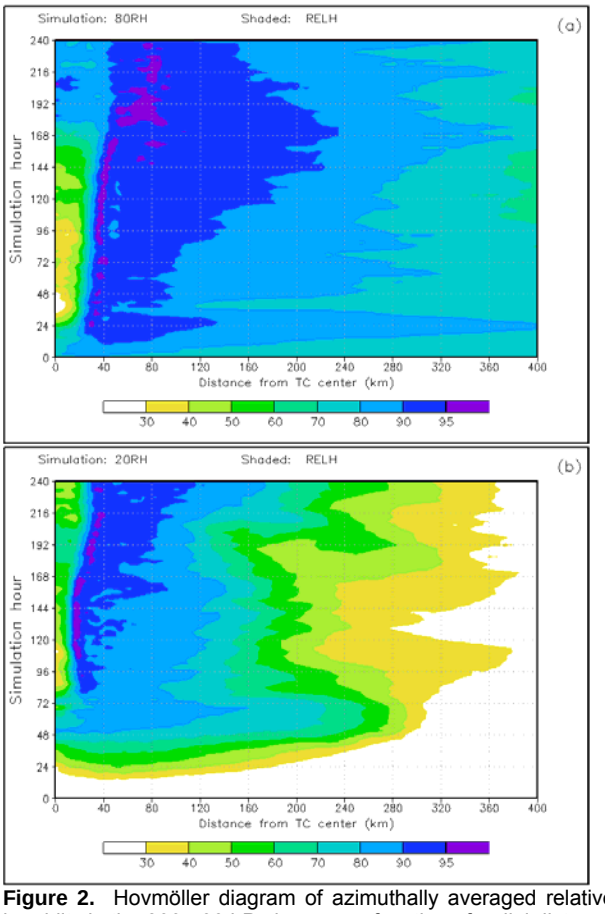

Figure 2. Hovmöller diagram of azimuthally averaged relative humidity in the 800-400 hPa layer as a function of radial distance from storm center: (a) 80RH simulation, (b) 20RH.

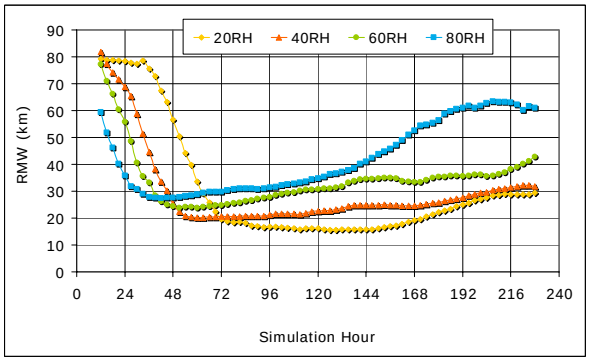

Figure 3. Time series of radius of maximum 10-m wind speed (km) with application of a 9-point smoother. Simulation name indicated in legend.

Azimuthal averages of 10-m wind speed with a bin size of 2 km were calculated, along with commonly used metrics for TC size such as the RMW and the radius of hurricane-force wind (hereafter RHFW). The RMW in all four simulations initially decreases from the ~80-km

initial condition value, exhibits a period of quasi-steady size, followed by an increase during the latter stages of the simulations (Fig. 3). *The RMW consistently equilibrates to a larger value in simulations with greater environmental humidity.* The RMW in the 20RH simulation is generally <20 km throughout the simulation, increasing to ~30-km near the end of the simulation, while the TC in the 80RH simulation exhibits a RMW that increases from ~30 km to >60 km during the simulation period.

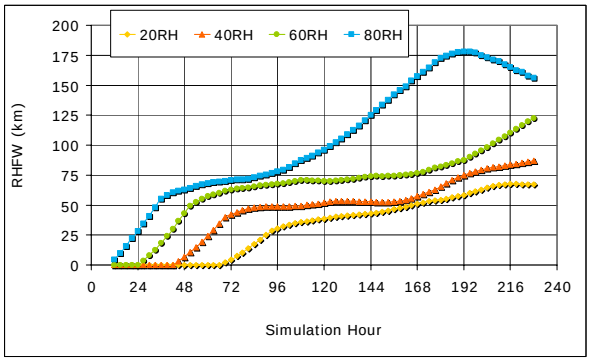

Figure 4. Time series of radius of hurricane force 10-m wind speed (km) with application of a 9-point smoother. Simulation name indicated in legend.

As with RMW, higher environmental humidity is also associated with larger RHFW values (Fig. 4). The TC in the 80RH simulation produces a maximum RHFW of ~175 km at hour 192, which is more than twice that seen in the 20RH and 40RH runs, and nearly double the 60RH value at that time. By the end of the simulation period, moistening in the initially drier simulations allows some convergence with the 80RH run.

We now examine the physical mechanism that is proposed to explain the size differences shown here. Figure 5 depicts the rainfall distribution, which is related to the size and strength of the cyclonic PV tower and the balanced primary circulation. Hovmöller diagrams of model-simulated composite radar reflectivity, with the RMW superimposed, reveal heavier precipitation in the 120-240-km radius belt in the 80RH run relative to the 20RH simulation (Fig. 5), as well as in the 40RH and 60RH runs (not shown). The eye wall, identified as the zone of highest reflectivity, is observed to expand to near 100 km in the 80RH run, while remaining closer to 40 km in the 20RH run.

The composite reflectivity at hour 168, which is a representative time for each run, is shown in Fig. 6. A broader eye wall and larger eye are evident in the 80RH run, along with heavier precipitation in the outer rainbands relative to the drier simulations. Progressively smaller eye sizes are found with decreasing environmental RH. Peak reflectivity values within the eye wall are comparable in each simulation, exceeding 55 dBz.

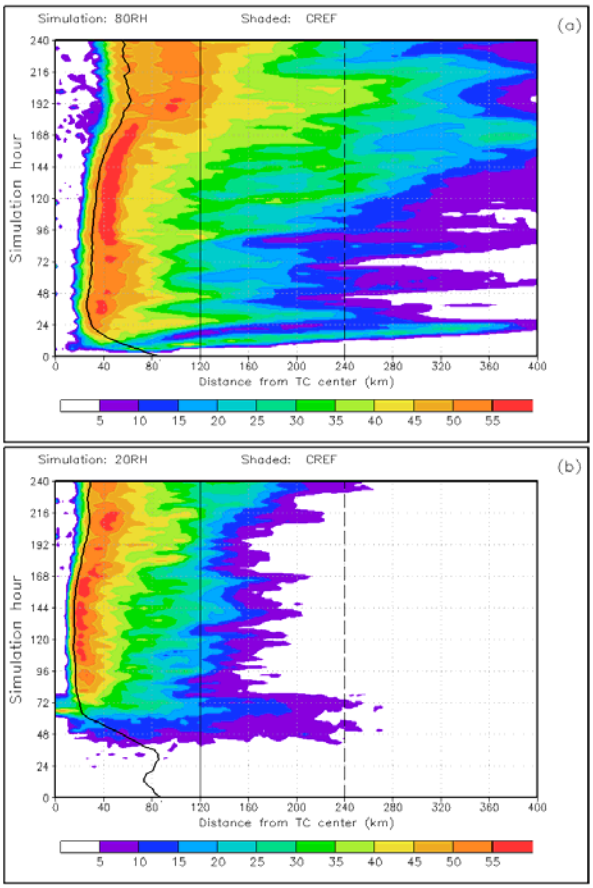

Figure 5. Hovmöller diagrams of composite simulated radar reflectivity (dBz): (a) 80RH, (b) 20RH. The 10-m RMW is shown by the thick black line, and radius values of 120 and 240 km are highlighted for reference.

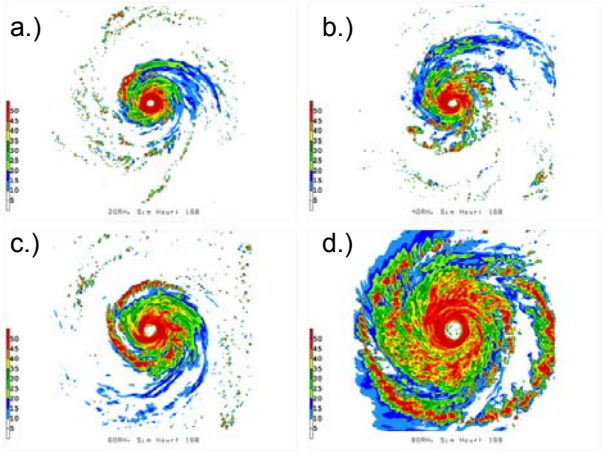

Figure 6. Model simulated composite reflectivity for hour 168: (a) 80RH, (b) 60RH, (c) 40RH, (d) 20RH.

For consistency with our hypothesis, expansion of the precipitation shield should be accompanied by an expansion in the PV tower and cyclonic wind field (RMW and RHFW). Hovmöller diagrams of 850-700 hPa PV illustrate that the PV tower expands to a radius of ~45 km in the 80RH run, while in the 20RH run the core of largest PV is restricted to a radius of ~25 km by the end of the simulation (Fig. 7). The RMW remains in a location immediately outside of the PV tower core, consistent with large values of both cyclonic shear and curvature vorticity inside this radius.

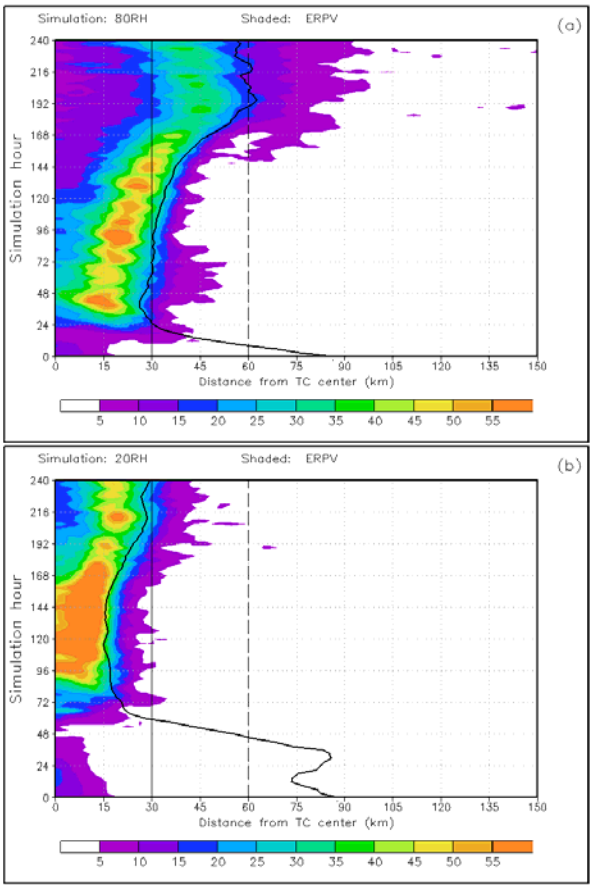

Figure 7. Hovmöller diagram of azimuthally and layer-averaged 850-700 hPa PV (PVU, 1 PVU = 10^{-6} m^2 s^{-1} K kg^{-1}). The radius of maximum 10-m wind speed is shown by the thick black line and radii of 30 and 60 km are highlighted for reference: (a) 80RH simulation, (b) 20RH.

The relation between precipitation and the PV field is shown in Fig. 8, which displays simulated composite reflectivity above a 46-dBz threshold superimposed on the 850-700 hPa PV contours. A close correspondence between the zone of heavy precipitation and the outer fringe of the PV tower is apparent in each simulation, and PV-tower expansion is observed to occur simultaneously or shortly after the lateral expansion of the region of heavy rainfall. The broader, weaker precipitation maximum in the 80RH run is consistent with the more diffuse PV tower evident late in this simulation (Fig. 8a).

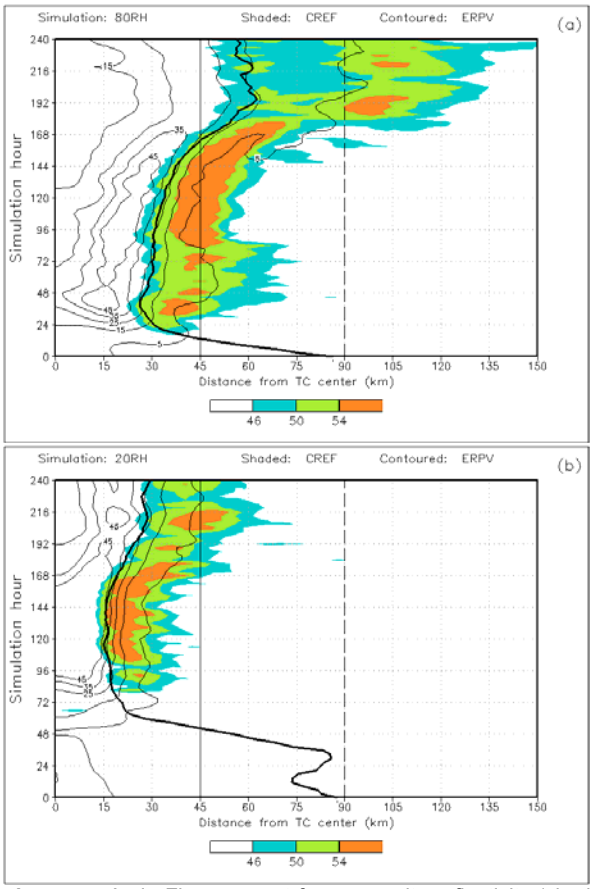

Figure 8. As in Fig. 7 except for composite reflectivity (shaded above 46 dBz) and average 850-700 hPa PV (contoured, PVU) after 2 passes with a 9-pt smoother.

The final step in linking the outer-core precipitation and PV tower expansion is to establish the relation between the diabatic (non-advective) PV tendency and the lateral growth of the PV tower. A PV budget, based on the methodology of Lackmann (2002), was calculated using output from the WRF simulations. A Hovmöller diagram showing the non-advective PV tendency in the 850-700 hPa layer, superimposed with contours of the PV in that layer (Fig. 9), demonstrates the expected relationship: the expansion of the PV tower is associated with strong non-advective PV generation near the outside edge of the PV tower. Diabatic PV generation is strongest and broadest in the more-moist simulations, since there is more precipitation in spiral rain bands outside of the eye wall in these simulations.

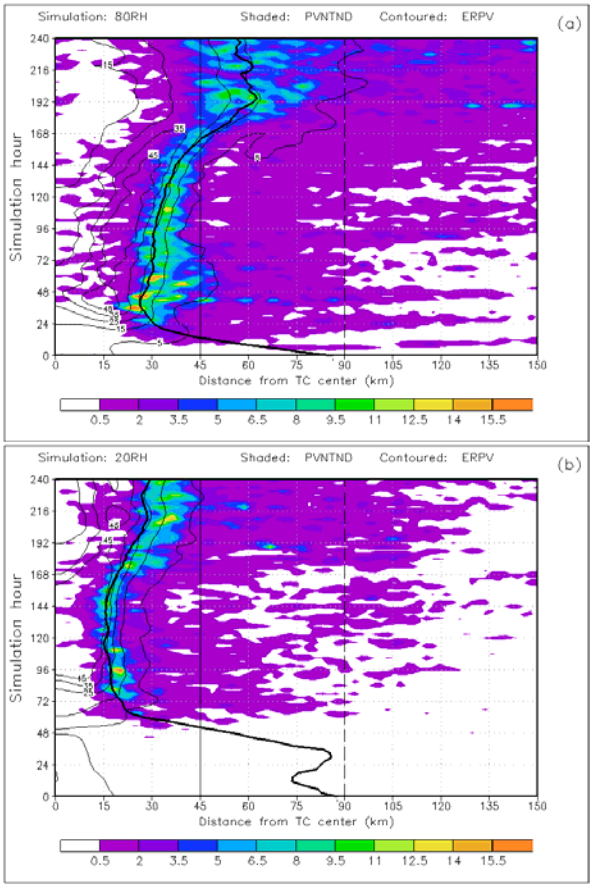

Figure 9. As in Fig. 7 except non-advective layer-average 850-700 hPa PV tendency (shaded, x 100 PVU s^{-1}) and PV (contoured). PV smoothed using 2 passes of a 9-pt smoother.

A strong correlation between the expansion of the RHFW and precipitation in the 150 km radial belt immediately outside the RMW is evident in both the 80RH and 20RH simulations (Fig. 10). This relation may hold implications for operational prediction of TC wind fields if observational studies are able to duplicate this relation.

4. CONCLUSION

We have advanced a simple hypothesis linking the lateral extent of the TC wind field to the intensity and distribution of precipitation outside the storm core, and in turn, to the environmental relative humidity. Idealized model experiments were used to test this idea, and the experimental results are consistent with the hypothesis. Simulations with higher initial relative humidity produced larger TCs, along with greater amounts of precipitation outside the eye wall, leading to greater diabatic generation of PV there, and subsequently larger PV towers and wind fields.

The use of idealized modeling to test our hypothesis is a first step towards a more comprehensive study. Future research should include analysis of observational data in order to determine if a correlation between environmental humidity (or outer-core precipitation) and TC size is evident. Satellite-derived surface wind measurements, such as those obtained from the QuikSCAT instrument, would facilitate such efforts. We have not yet examined the sensitivity of TC size to humidity at different altitudes; this information could be potentially useful in an operational environment.

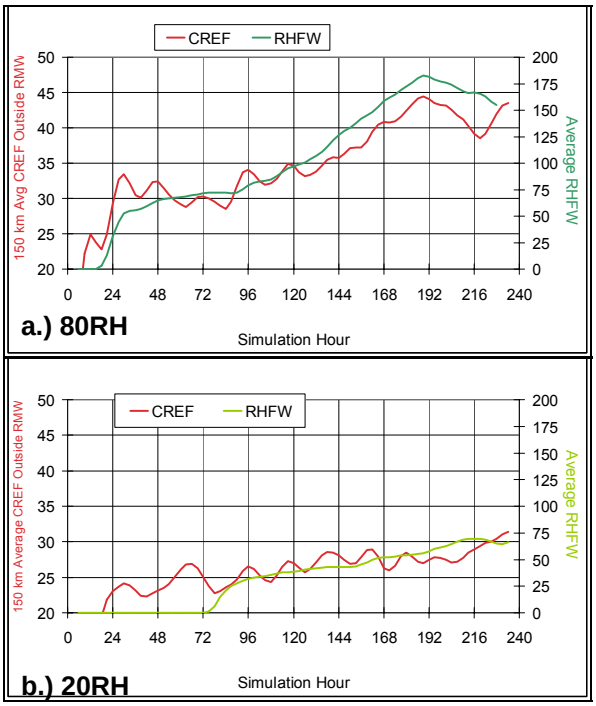

Figure 10. Time series of average composite reflectivity in 150-km annulus outside of RMW and average RHFW: (a) 80RH, (b) 20RH.

The results of this study suggest that examination of relative humidity fields from model analyses and forecasts could provide information about possible differences or changes in the size of a TC wind field. If increases in outer-core precipitation are found to precede wind field expansion, it may be possible to derive operational benefits. Satellite imagery could be used to monitor the extent of precipitation outside the storm core, which might facilitate anticipation of TC wind-field expansion. Interactions with fronts or mid-latitude troughs during extratropical transition could indicate that wind-field expansion is imminent if precipitation is observed to increase in the outer core of the storm.

Acknowledgements. This research was supported by NSF grant ATM-0334427, and DOE grant ER64448, both awarded to North Carolina State University. The WRF model was made available through NCAR, sponsored by the NSF. Some of the WRF model simulations were performed at the Renaissance Computing Institute (RENCI), which is supported by UNC Chapel Hill, NCSU, Duke University, and the state of North Carolina.

References

Atkinson, G. D., 1971: Forecaster's guide to tropical meteorology. Tech. Rep. 240, Air Weather Service, Scott Air Force Base, IL 62225, 295 pp.

Cocks, S. B., and W. M. Gray, 2002: Variability of the outer wind profiles of Western North Pacific typhoons: Classifications and techniques for analysis and forecasting. *Mon. Wea. Rev.,* **130,** 1989–2005.

Emanuel, K. A., 1986: An air-sea interaction theory for tropical cyclones. Part I: Steady-state maintenance. *J. Atmos. Sci.*, **43**, 585–604.

Frank, W. M., and W. M. Gray, 1980: Radius and frequency of 15 m s^{-1} (30 kt) winds around tropical cyclones. *J. Appl. Met.,* **19,** 219–223.

Hill, K. A., and G. M. Lackmann, 2008: Analysis of idealized tropical cyclone simulations using the Weather Research and Forecasting Model: Sensitivity to turbulence parameterization. *Mon. Wea. Rev.* **136,** *in press*.

Hong, Y.-Y., and J.-O. J. Lim, 2006: The WRF single-moment 6-class microphysics scheme (WSM6). *J. Korean Meteor. Soc*., **42**, 129–151.

Janjić, Z. I., 2002: Nonsingular implementation of the Mellor-Yamada Level 2.5 Scheme in the NCEP Meso model. *NCEP Office Note,* **No. 437,** 61 pp.

Jordan, C. L., 1958: Mean soundings for the West Indies area. *J. Meteor.*, **15,** 91–97.

Kimball, S. K., 2006: A modeling study of hurricane landfall in a dry environment. *Mon. Wea. Rev.,* **134,** 1901–1918.

Kimball, S. K., M. S. Mulekar, 2004: A 15-year climatology of North Atlantic Tropical Cyclones: Part I: Size parameters. *J. Climate,* **17,** 3555–3575.

Lackmann, G. M., 2002: Cold-frontal potential vorticity maxima, the low-level jet, and moisture transport in extratropical cyclones. *Mon. Wea. Rev.,* **130,** 59–74.

Merrill, R. T., 1984: A comparison of large and small tropical cyclones. *Mon. Wea. Rev.,* **112,** 1408–1418.

Rotunno, R. and K. A. Emanuel, 1987: An air-sea interaction theory for tropical cyclones. Part II: Evolutionary study using a nonhydrostatic axisymmetric numerical model. *J. Atmos. Sci.*, **44**, 542–562.

Skamarock, W. C., J. B. Klemp, J. Dudhia, D. O. Gill, D. M. Barker, W. Wang, and J. G. Powers, 2007: A description of the advanced research WRF Version 2. *NCAR Technical Note.*